Published in final edited form as:
Mater Sci Eng C Mater Biol Appl. 2011 January 1; 31(1): 22–29. doi:10.1016/j.msec.2010.04.001.

Impact of Scaffold Micro and Macro Architecture on Schwann Cell Proliferation under Dynamic Conditions in a Rotating Wall Vessel Bioreactor

Chandra M. Valmikinathan, **John Hoffman**, and **Xiaojun Yu**
Department of Chemistry, Chemical Biology and Biomedical Engineering Stevens Institute of Technology, Hoboken, NJ, 07030

Abstract

Over the last decade tissue engineering has emerged as a powerful alternative to regenerate lost tissues owing to trauma or tumor. Evidence shows that Schwann cell containing scaffolds have improved performance in vivo as compared to scaffolds that depend on cellularization post implantation. However, owing to limited supply of cells from the patients themselves, several approaches have been taken to enhance cell proliferation rates to produce complete and uniform cellularization of scaffolds. The most common approach is the application of a bioreactor to enhance cell proliferation rate and therefore reduce the time needed to obtain sufficiently significant number of glial cells, prior to implantation.

In this study, we show the application of a rotating wall bioreactor system for studying Schwann cell proliferation on nanofibrous spiral shaped scaffolds, prepared by solvent casting and salt leaching techniques. The scaffolds were fabricated from polycaprolactone (PCL), which has ideal mechanical properties and upon degradation does not produce acidic byproducts. The spiral scaffolds were coated with aligned or random nanofibers, produced by electrospinning, to provide a substrate that mimics the native extracellular matrix and the essential contact guidance cues.

At the 4 day time point, an enhanced rate of cell proliferation was observed on the open structured nanofibrous spiral scaffolds in a rotating wall bioreactor, as compared to static culture conditions. However, the cell proliferation rate on the other contemporary scaffolds architectures such as the tubular and cylindrical scaffolds show reduced cell proliferation in the bioreactor as compared to static conditions, at the same time point. Moreover, the rotating wall bioreactor does not alter the orientation or the phenotype of the Schwann cells on the aligned nanofiber containing scaffolds, wherein, the cells remain aligned along the length of the scaffolds. Therefore, these open structured spiral scaffolds pre-cultured with Schwann cells, in bioreactors could potentially shorten the time needed for grafts for peripheral nerve regeneration.

Keywords

Peripheral Nerve Regeneration; Spiral Shaped Scaffolds; Rotating wall bioreactor; Schwann cell; Aligned nanofibrous scaffolds

Corresponding Author: **Dr. Xiaojun Yu, Ph.D.** Assistant Professor Department of Chemistry, Chemical Biology and Biomedical Engineering Stevens Institute of Technology Hoboken, NJ, 07030 USA xyu@stevens.edu Phone: 201 216 5256 Fax : 201 216 8306.

Introduction

With an ever increasing demand for grafts to bridge peripheral nerve gaps, the need for an ideal scaffold for enhanced regeneration is necessary [1,2,3]. Despite the early promise of tissue engineering, researchers have faced challenges in regenerating peripheral nerve tissues over large gaps (exceeding 4 mm) [1,2,4]. Current tissue engineering approaches investigate the use of bioactive or bioresorbable matrices, which rely on the appropriate cellular response *In Vivo*, with the development of biological and physical functionality post implantation [5,6]. A limitation of this approach is the inconsistency of the host response in terms of resorption, recellularisation and regeneration, which can result in development of inappropriate regeneration parameters, and hence failure of the implanted graft to perform its role of regeneration [7,8]. Several tissue engineering strategies have served as alternatives to bridge nerve gaps. However, none of these approaches match levels of regeneration achieved by autografts [4,9]. Evidence suggest that the reason could be due to the availability of large amounts of viable support (glial) cells and conducive growth cones mimicking the site, prior to injury [10].

In the case of peripheral nerve regeneration and tissue engineering, evidence indicates that grafts seeded with Schwann cells prior to implantation have shown enhanced nerve regeneration in vitro and in vivo [11]. Schwann cell migration into the channels is known to be a critical factor for peripheral nerve regeneration [12]. When Schwann cells were seeded into nerve guidance channels, the injured peripheral nerves regenerated at a faster rate and over longer distances [13]. The success of Schwann cells in peripheral nerve regeneration results in part from their production of the cell adhesion molecules and neurotrophic factors, which mediate the neurite attachment and growth. However, the time needed for growing sufficient numbers of autologous Schwann cells for seeding into guidance channels is unacceptably long as this often allows the injury to worsen [14]. Also, while obtaining cells from the patients themselves, acquiring large amounts of cells is not possible. Hence, bioreactors provide a viable opportunity for fast and large scale multiplication of cells in vitro.

The rotating wall bioreactor, developed by NASA, is a form of dynamic culture system, designed to utilize low shear, three-dimensionality, and high mass transfer to promote *ex vivo* tissue synthesis [15,7]. The dynamic culture approaches in rotating bioreactors have been proposed to provide a well-mixed environment and possible culture medium flow within and around 3D scaffolds during cultivation, and thus improve nutrient supply and expedite the efflux of cytotoxic degradation and metabolic waste products produced by cells [15,16]. Lin et.al. have showed that a rotating wall bioreactor can be employed to study the proliferation and differentiation of neural stem cells on collagen based carriers, that were about 1 mm in diameter [17]. Enhanced cell proliferation and differentiation was observed at the two week time point and more importantly, the absence of a necrotic cell core, owing to enhanced mass transport into spherical particles, was observed. This can be attributed to the fact that the carriers they used were small spherical collagen based particles that were exposed to medium exchange from 3 dimensions. However, traditional tissue engineering approaches to peripheral nerve regeneration employs cylindrical or tubular “closed” scaffolds with diminished surface area and reduced mass transport into the scaffold.

We had earlier shown the development of scaffolds with spiral architecture, with uniform wall and gap parameters, in order to alleviate some of the drawbacks associated with contemporary geometries[18]. In the previous study, the scaffolds were fabricated by sintering poly (lactide-co-glycotide) (PLGA) microparticles. Even though this system provided scaffolds with optimal porosity, pore interconnectivity and mechanical properties, they were slightly brittle and hard to shape into desired spiral architectures and therefore

needed higher temperatures to shape them into desired 3 dimensional architectures. It is also known that PLGA yields acidic byproducts on degradation, which induce macrophage response upon in vivo implantation [19]. On the other hand, polycaprolactone (PCL) has increased modulus and hence can be shaped easily into complex architectures and also does not produce byproducts that are acidic. It is also known that the processing temperature for the PCL using this technique does not need elevated temperatures and therefore are ideally suited in cases where temperature sensitive proteins, such as growth factors, need to be included in the matrix[20]. Also, recent evidence indicate that PCL based phase separated thin films and electrospun nanofiber scaffolds promote Schwann cell attachment and proliferation evaluated over short and long durations [21]. The stydy also suggested that the PCL based scaffolds allowed for Schwann cells to exist in a spindle like morphology, meanwhile the other materials tested inhibited such morphologies. More importantly, Pierucci et.al., showed that PCL based scaffolds showed significantly enhanced axonal growth and Schwann cell proliferation as compared to Poly (L-Lactide) (PLLA) based scaffolds, upon in vivo implantation in a rat sciatic defect model [22].

Based on the above findings we have developed nanofiber coated phase separated PCL based spiral scaffolds for peripheral nerve regeneration. Specifically, we evaluate the impact of scaffold geometry (spiral, cylindrical and tubular) on cell proliferation under dynamic culture conditions, by culturing Schwann cells in a rotating wall bioreactor. We hypothesize that the open architecture of the spiral scaffolds could provide better media influx into the scaffold, therefore enhancing cell proliferation as compared to other contemporary scaffold architectures. We also seek to evaluate the effect of dynamic culture conditions on scaffold microarchitecture such as nanofiber coating and alignment on the surface of the scaffold.

Materials and Methods

2.1. Materials

Main chemicals used for scaffold preparation including polycaprolactone (PCL) and N,N-dimethylacetamide (DMac)were purchased from Sigma-Aldrich, 1,1,1,3,3,3-hexafluoro-2-propanol (HFIP, Oakwood Products), and dichloromethane (DCM, Parmco-Aaper), were used as received. All cell culture reagents including Dulbecco's modified eagle medium (DMEM), fetal bovine serum (FBS), penicillin streptomycin, and trypsin were purchased from Mediatech. Analytical reagents include 3-(4, 5-dimethylthiazol-2-yl)-5-(3-carboxymethoxyphenyl)-2-(4-sulfophenyl)-2H-tetrazolium (MTS) and phenazine methosulfate (PMS) from Promega Corporation.

2.2. Scaffold fabrication

2.2.1. Preparation of cylindrical and tubular scaffolds—The porous polymeric cylindrical and tubular scaffolds were fabricated via a previously described phase inversion and salt leaching technique [23]. Briefly, a 20% (w/v) PCL in DMac solution was stirred for 2 hours at 52°C. Sodium chloride (150-200 μm, Fischer Scientific) was added as a crystal porogen at 25% (w/w to PCL) to the polymer solution and thoroughly mixed. The resulting suspension was then cast into a 5 mm thick Teflon mold with 5 mm diameter circular holes to produce the cylindrical scaffolds. Teflon tubes (McMaster-Carr) 3 mm in diameter were aligned to the center of the cylinders to provide the confines for the tubular scaffolds. The solvent was then extracted from the PCL constructs via immersion in 70% ethanol (Fisher Scientific) at room temperature. The scaffolds were further submerged in deionized water for 48 hours with periodic water replacement in order to remove residual solvent as well as leach the salt away.

2.2.2. Preparation of PCL spiral scaffolds—Four different spiral constructs were prepared and used in this study. They were PCL based spiral scaffolds, (1) without salt, (2) with salt, (3) with salt and a random nanofibrous PCL coating, and (4) with salt in addition to an aligned nanofiber coating. The spiral scaffolds were prepared using the salt-leaching method reported previously by Kong et.al. [23]. Briefly, 25% (w/w) of salt was added to a polymeric solution of 33% PCL in DCM and mixed thoroughly. In preparing the non-salt PCL spirals, salt was instead simply not incorporated into the polymeric PCL solution. The resultant solution was poured as a thin layer onto a Petri dish to form a 2 mm thick PCL sheet. The polymeric sheet was then vacuum-dried overnight to remove the DCM solvent.

For the corresponding nanofiber-coated PCL scaffolds, a polymeric solution of 8% PCL in HFIP was electrospun directly onto both sides of the PCL sheet using a custom electrospinning configuration. Specifically, the fibers were collected from a positively-charged vertical needle onto a stationary PCL sheet situated on a grounded horizontal aluminum foil. In order to acquire an aligned nanofibrous coating, the electrospinning configuration was modified to include a mandrel rotating at 80 rpm situated between the metal capillary and the zero potential aluminum foil. A flow rate of 10 μL / min and a working distance of 10 cm between the collector and the spinneret (needle) were maintained in both cases.

Rectangular strips measuring 5 mm in width and 4 cm in length were then cut from the PCL sheets. In order to fix the strips into the desired spiral geometry with three cycles, the PCL strips were rolled along a thin copper sheet acting as a mold in-between adjacent layers. The spiral structure was stabilized by heating the scaffolds to 45 °C for 30 minutes, followed by freezing at −20°C in order to facilitate the extraction of the tightly wound scaffolds from the copper encasing.

2.3. Scaffold Characterization

2.3.1 Porosity measurements—The porosity (P) of the scaffolds was calculated by gravimetry based on the inherent density of the PCL material (p_{mat}) and the density of the scaffold (p_{sc}) according to the equation: $P = (1-p_{sc}/p_{mat})$. The scaffold density was determined by dividing the mass of a scaffold by the volume of water it displaced. At least six scaffolds per sample type was evaluated for porosity using the gravimetry technique.

2.3.2 Optical and Scanning Electron Microscopy—The spiral scaffolds were initially assessed with a Nikon SMZ1500 Light Microscope to observe the overall geometry of the scaffolds. The surface morphology of the polymeric scaffolds and fiber alignment was qualitatively analyzed with a Philips Leo 982 FEG SEM. All SEM specimens were dried in a vacuum dessicator, gold coated, and imaged at accelerating voltages of 1-3 kV and working distances of 4-9 mm.

2.4. In vitro study

Rat Schwann cells (ATCC, MD) was used as the cell line to test the attachment and proliferation of cells on the scaffolds. Schwann cells were maintained in Dulbecco's modified eagles medium (DMEM) supplemented with 10 % fetal bovine serum (FBS, ATCC, MD) and 1 % Penicillin Streptomycin (Invitrogen). The cells were cultured in an incubator with 5% CO2 and a relative humidity of 95 %.

2.4.1 Cell proliferation assay—Prior to seeding, the scaffolds were sterilized in 70% ethanol for 30 minutes, irradiated by UV light in sterile phosphate-buffered saline (PBS) for one hour, and then soaked in serum free media for ten minutes to enhance wettability and facilitate cell attachment. The cylindrical and tubular scaffolds, as well as the four

aforementioned spiral configurations, were placed at the bottom of 24-well plates. Rat Schwann cells were then seeded at a density of 1×10^5 cells per scaffold in 100 μL media suspension and placed into a 5% CO_2 incubator at 37°C for two hours. Following this, 2 ml fresh complete media was added to the scaffolds and the scaffolds were cultured for 1 day. At the end of this time point the cell attachment on the scaffold was evaluated using a tetrazolium compound (3-(4,5-dimethylthiazol-2-yl)-5-(3-carboxymethoxyphenyl)-2-(4-sulfophenyl)-2H-tetrazolium, inner salt) (MTS) assay as described in the next section.

For a longer duration study, after the attachment (day 1), half of the scaffolds were either transferred to a bioreactor for dynamic culture or left in the tissue culture plates, with medium to provide a static growth environment for the Schwann cells. For the dynamic conditions, the scaffolds were transferred to a rotating wall vessel bioreactor and rotated at 30 RPM and the scaffolds were maintained in 50 ml complete medium for 4 days. At the end of 4 days, the scaffolds were retrieved and characterized for cell proliferation using MTS assay and morphologically using confocal and electron microscopy. The cell proliferation on scaffolds, maintained under dynamic conditions was compared against scaffolds with cells cultured under static conditions at the same time point.

2.4.2. Cell quantification—The proliferation of the Schwann cells were quantified via MTS assay (1:20 0.9% PMS/MTS) after day 1 and day 4 to assess cell adhesion and proliferation kinetics, respectively. In brief, 250 μL of analytical reagent consisting of a 1:20 ratio of PMS (.9 mg/mL in PBS) to MTS (2mg/mL in PBS) was added to the appropriate wells and incubated for 3 hours. The absorbance values were recorded at 490 nm using a microplate-reader (Biotek).

2.4.3. Confocal and scanning electron microscopy—Scaffolds seeded with Schwann cells after different time intervals (1, 4 days) were fixed in 4% paraformaldehyde overnight, and then washed with PBS. Prior to imaging with a Nikon C1 confocal microscope, the scaffolds were sectioned into small pieces, incubated with primary anti S-100 (1:100 in PBS, Sigma), and then stained with anti-mouse Texas red secondary antibody. The confocal images were primarily used to assess the orientation response of cells based on the underlying surface morphology of the scaffold (e.g. aligned nanofiber coating) as well as to study the cell proliferation and phenotype on the spiral scaffolds owing to dynamic conditions. As for imaging via SEM, the same protocol followed above (*2.3.2*) was repeated after the cells were fixed and the scaffolds were cut into smaller specimens.

2.4 Statistical analysis

All quantitative data are reported as mean ± standard deviation. At least 3 samples per time point per scaffold type were evaluated for statistical analysis. Statistical differences among the groups of scaffolds were determined by performing a student's t test. A confidence interval of $p < 0.05$ was considered to be statistically significant.

Results and Discussions

3.1 Spiral scaffold architecture

The geometry of the spiral scaffolds is conceptualized in an isometric view with Solid Works® in Figure 1. The key parameters of the scaffold include wall thickness, gap distance, diameter and height. The gap distance is dependent upon the thickness of the copper mold used to maintain the spiral structure, whereas the wall thickness is controlled by the volume and concentration of the PCL solution used to fabricate the salt-leached polymeric sheets. The number of revolutions and height is dictated by the rectangular geometry cut from the PCL sheets, which in this particular setup measures 4 cm by 5 mm.

Thus, the fabricated spiral scaffolds is characterized by 3 revolutions with a wall thickness of 600um, gap distance of 200 μm, and height of 5 mm. Theoretically, the surface area of the spiral scaffold is 4.54 cm^2, which is a 300% increase as compared to the surface area of the tubular control (1.51 cm^2) with an inner and outer diameter of 3mm and 5mm, respectively.

The porosity of the scaffolds was determined via a gravimetric method based on the volume of water displaced by a scaffold of known mass. The scaffolds incorporated in the porosity analysis (n=3) included spiral scaffolds without salt (SN), with salt (SS), with salt and random nanofibers (SS-R), and with salt and aligned nanofibers (SS-A), as well as cylindrical (CL) and tubular (TL) scaffolds for control. The incorporated NaCl crystals have a diameter ranging 150-200 μm, and consequently, the SS, SS-R, and SS-A as well as the cylindrical and tubular scaffolds have pore sizes flanking this magnitude.

Native acellular nerve grafts have a porosity of approximately 70% [24] and from Figure 2 we can see that all scaffolds had a porosity ranging from 75% to 84% except for the SN scaffold, which had a significantly lower porosity of 26%. The application of nanofibers onto the surface of spiral scaffolds was shown to slightly decrease the porosity with increasing levels of orientation. This relationship with fiber alignment was not statistically significant ($p < 0.05$) due to the relatively low volume of nanofibers with respect to the entire volume of the composite scaffold. However, the observable porosity change due to a minute volume emphasizes the difference of porosity between the PCL nanofiber and PCL scaffold, and between nanofiber mats with different levels of alignment.

3.2 Spiral morphology

Optical microscopy images were acquired to initially assess the architecture of the fabricated spiral, cylindrical and tubular scaffolds. As it can be seen from figure 3, spiral architecture with uniform wall and gap parameters could be fabricated by our technique. The surface topography of the porous scaffolds were further characterized by SEM. Figure 4 shows scaffold pore geometry with porous architecture in the walls. It can also be evaluated, from Figure 4B, that the pore size was in the range of 100 and 150 microns with uniform and interconnected pores, ideal for cell attachment and migration into the scaffolds. It can also be evaluated from figure 4C and figure 4D that various nanofiber alignments can be created on the scaffolds , with figure 4C showing random distribution of electrospun fibers on an SS-R scaffold and 4D showing aligned morphology on the nanofibers on the SS-A scaffold. Also, the uniform nanofiber coating on the substrate shows complete coverage and structures mimicking the native extracellular matrix.

3.3 Cell adhesion and proliferation

3.3.1 Function of gross geometrical shape and porosity—Schwann cells were cultured on the scaffolds to provide a preliminary assessment of cellular response according to the scaffold architecture and nanofibrous topography in both static and dynamic environments. Cell adhesion and proliferation were determined via MTS assay, with cell attachment kinetics being associated to MTS readings taken one day after the initial seeding, and proliferation linked to the readings acquired four days post-seeding. Figure 5 is acompilation of the MTS assays (n=3) attachment profiles (day 1) for different scaffolds (CL, TL, SN, SS, SS-R, SS-A) cultured in a traditional static environment (i.e. culture plates).

As shown in Figure 5, an increase in surface area enhances the cellular adhesion and proliferation. The MTS absorbance from the porous SS scaffolds was higher than those registered by the cylindrical (CL) and tubular (TL) scaffolds for day 1. Though the

difference was statistically significant ($p<0.05$), it is evident that there does not exist a linear relationship between surface area and number of cells that attach to the scaffold. Figure 5 also demonstrates the importance of incorporating a porous matrix in promoting cellular growth kinetics. The porous spiral scaffolds (SS) registered higher absorbance values ($p< 0.05$) than non-porous spiral scaffolds (SN), whose porosity was previously shown to be only one-thirds of that of all the other scaffolds developed by salt-leaching. Therefore, we conclude, the porous topography increases the focal points to which cells can attach, while the underlying porous network allows greater cellular invasion as well as nutrient exchange.

Also, on examining the effect on cellular response due to the addition of nanofibers, it can be understood that cellular adhesion (day 1 MTS assay) were enhanced significantly ($p<0.05$) on nanofiber coated spiral scaffolds (both random and aligned). However, random fibers measured higher cell densities than aligned nanofibers on day 1 post-seeding. This contradiction can be explained due to the difference in surface roughness between the two nanofibrous mats. The roughness of the nanofibrous mats differ appreciably, with the aligned nanofibers ultimately having a much smoother topographical profile. A smoother profile suggests that fewer sites for surface-cell interactions are available, and therefore SS-A yields lower cellular adhesion than SS-R.

Similar results have been observed by Fonner JM et.al [25], where an increase in surface roughness was accompanied by enhanced Pheochromocytoma 12 (PC12) and Schwann cell attachment and proliferation rates. Pennisi CP et.al. also observed an increased fibroblast and glial cell attachment and proliferation on surfaces with increasing roughness for nanostructured platinum based neural electrodes [26]. Several other reports have also suggested similar outcomes, especially for other cell types, commonly used in tissue engineering, specifically, osteoblast and fibroblast cells [27]. Erisken et.al., have showed that with an increasing nanofiber density and increasing surface roughness was observed, which also affected the osteoblast cell attachment and proliferation [28].

3.3.3 Functional performance in dynamic culture—The effect of a dynamic environment with respect to a static culture was also examined in terms of cell proliferation, morphology and cell phenotype. An evident trend was discernable wherein all spiral scaffolds had improved cell numberswhen cultured in a rotating bioreactor (30 rpm) as compared to static culture conditions. Meanwhile, cylindrical and tubular scaffolds (CL and TL) showed reduced cell proliferation rate when subjected to dynamic conditions as compared to static culture conditions, as shown in figure 6. Similar observations have been reported in other studies, where reduced number of cells were observed on cylindrical scaffolds when culture on rotating wall bioreactor as compared to static conditions [29]. Thus, we conclude, the spiral scaffolds exhibited improved functional performance as compared to the other geometries when dynamic conditions, paralleling the physiological environment, were emulated.

Moreover, the spiral walls are thinner than the walls of the tubular and cylindrical scaffolds and are subjected to cellular invasion from both sides of the wall, and hence, have greater ratio of interior to exterior cells than the other scaffolds. Though tubular walls are also subjected to cellular penetration from two opposing surfaces (inner lumen to outer wall), the thickness is greater at 1mm, therefore preventing complete cellularization across the scaffold. Also, the open architecture of the spiral scaffolds enhances the nutrient transport and waste removal, thereby promoting the viability of interior cells, it is no surprise that the cell density on the spiral scaffolds was enhanced by dynamic flow, whereas tubular, and to a greater extent, cylindrical scaffold cell counts were decreased.

Also, from figure 6 it is evident that the nanofiber coating on the spiral scaffolds enhanced cell proliferation in the static as well as dynamic conditions for day 4 as compared to other scaffolds. This elucidates the fact that the nanofibers mimic the native ECM and provide enhanced surface areas for cell proliferation. It can also be observed that the aligned nanofibers have enhanced cell proliferation as compared to random nanofibers, especially when subjected to dynamic conditions. This can be attributed to the impact of contact guidance and key role it plays in scaffold maturation and providing an ideal microenvironment for neuronal tissue development.

Similar results have been shown with rotating wall bioreactor for several tissues including cartilage, bone and even for neuronal systems. [30,31,17] Botchwey et.al., used a rotating wall bioreactor to enhance cell seeding efficiency and to study matrix formation using microsphere based carrier matrices for bone tissue engineering [32]. They observed that the cell numbers increased on the scaffolds with time, and also observed a matrix formation composed of nodules of fiber and ceramic like architectures. Freed et.al., showed similar results on Polyglycolic acid based discs for cartilage regeneration[33]. They observed that the cells numbers, matrix production, as estimated by collagen II and glycosaminoglycans (GAG) were all enhanced when cultured in a rotating wall bioreactor as compared to static culture conditions. On the contrary, Mikos et.al, showed that with culture in a rotating wall bioreactor, cell numbers as well as the matrix mineralization and alkaline phosphatase activity was reduced as compared to static culture conditions, for very similar scaffolds, cells and culture conditions [29]. They also suggested that when examined, these scaffolds showed almost no cell proliferation, matrix mineralization within the scaffolds, even when cultured in a rotating wall bioreactor. This result has been confirmed in this publication, where reduced cell numbers were observed on cylindrical scaffolds and tubular scaffolds, when cultured in a rotating wall bioreactor as compared to static conditions, therefore warranting the need for alternative scaffold architecture, with a higher open surface area for media influx.

Scanning electron micrographs of the nanofiber-coated spirals were acquired to determine the effects of nanofiber alignment on cell morphology under dynamic culture conditions. As evident from Figure 7A, random fibers induced non-directed spreading of Schwann cells across multiple fibers. Meanwhile, the aligned nanofibers (figure 7B) induced cell spreading along the fiber orientation and formation of cell clusters around the nanofiber matrix.

Confocal images were obtained to confirm the effect of fiber orientation in the case of cells under static and dynamic conditions on nanofiber coated spiral scaffolds. Figure 8A shows Schwann cell proliferation on aligned nanofibers on day 4. From the figure it is evident that the cells oriented along the direction of the nanofibers. Figure 8B shows the image of aligned nanofiber containing spiral scaffolds when subjected to dynamic conditions. From the images, it is evident that the shear conditions and the rotation of the vessel did not have any impact on the orientation of the cells on the scaffolds and an increased number of cells can be seen on the scaffolds as compared to static conditions. Based on calculation by Botchwey et. al [32] and Cui et.al34, it can be identified that a linear relationship exists between the particle radius and the shear stress acting on the surfaces. A linear calibration was identified as given by the equation below.

$$\text{Shear stress}\,(\tau) = 0.0005 \times R_p$$

where R_p is the particle radius, in microns. All the calculations were made based on single particles suspended in medium rotating at a constant velocity in a rotating wall bioreactor. In our calculations however the particle size is the scaffold size, with wall thickness in the

range of 500 to 600 microns. Based on this the stress can be identified as 0.3 N/m^2. It is well understood that for mammalian cells, the shear stress should in the range of 0.3-1 N/m2, beyond which severe damage to cells would occur, causing reduced cell proliferation rates and even cell death35. Our calculations indicate that the shear stress on our spiral walls are in the lower limit of this range, therefore minimal if any damage would occur.

Figure 8 C indicates complete cellularization of the aligned nanofiber containing scaffolds as expected due to exposure to dynamic conditions. Also, no significant phenotype changes were observed, indicative of the fact that the mild shear conditions do not have an impact on the cells. This is confirmed by the fact that Schwann cells stained positive for S-100 antibody, which is a traditional marker to confirm presence of Schwann cells either microscopically or using a western blot analysis. Also, there was no significant difference in the S-100 expression in the case of static or dynamic culture conditions at the same time point or different time points (days 1 and 4).

4. Conclusions

In this study, a porous spiral-shaped scaffold was fabricated via solvent casting and salt-leaching and was coated with aligned and random PCL nanofibers serving as an ECM analog. Porous PCL serves as the spiral wall and provides mechanical strength as well as the three dimensional architecture for matrix development and the nanofibrous coating serves to provide guidance cues to direct Schwann cell orientation and enhance glial cell adhesion and proliferation. The open spiral scaffolds promoted enhanced Schwann cell attachment and proliferation, under dynamic conditions, as compared to static culture conditions at the same time point. Also, no significant changes in the cell phenotype were observed. More importantly, cell proliferation was significantly higher on spiral scaffolds with respect to cylindrical and tubular scaffolds, which had reduced cell numbers under dynamic conditions as compared to static conditions. Based on these findings, we conclude that nanofiber containing spiral open scaffolds, pre-seeded with Schwann cells and cultured in a rotating wall bioreactor could potentially provide alternatives to bridge peripheral nerve gaps comparable to the levels of regeneration achieved by autografts.

Acknowledgments

The authors would like to thank the National Institute of Health (R03 NS058595) for funding this research.

References

1. Belkas JS, Midha R, Shoichet MS. Restorative Neurology And Neuroscience. 2005; 23:19–29. [PubMed: 15846029]
2. Belkas JS, Shoichet MS, Midha R. Neurol. Res. 2004; 26:151–160. [PubMed: 15072634]
3. Battiston B, Geuna S, Ferrero M, Tos P. Microsurgery. 2005; 25:258–267. [PubMed: 15934044]
4. Yu X, Bellamkonda RV. Tissue Eng. 2003; 9:421–430. [PubMed: 12857410]
5. Siemionow M, Sari A. Neurol. Res. 2004; 26:218–225. [PubMed: 15072642]
6. Nicoli-Aldini N, Fini M, Rocca M, Giavaresi G, Giardino R. Int. Orthop. 2000; 24:121–125. [PubMed: 10990379]
7. Eiselt P, Kim BS, Chacko B, Isenberg B, Peters MC, Greene KG, Roland WD, Loebsack AB, Burg KJL, Culberson C, Halberstadt CR, Holder WD, Mooney DJ. Biotechnology Progress. 1998; 14:134–140. [PubMed: 9496678]
8. Goldstein AS, Christ G. Tissue Engineering Part A. 2009; 15(4):739–740. [PubMed: 19292675]
9. Dodla MC, Bellamkonda RV. Biomaterials. 2008; 29(1):33–46. [PubMed: 17931702]
10. Chew SY, Mi R, Hoke A, Leong KW. Biomaterials. 2008; 29(6):653–661. [PubMed: 17983651]
11. Wiberg M, Terenghi G. Tissue Eng. 2001; 7:525–534. [PubMed: 11694187]

12. Hoke A. Nature Clinical Practice Neurology. 2006; 2(8):448–454.
13. Hadlock TA, Sundback CA, Hunter DA, Vacanti JP, Cheney ML. Microsurgery. 2001; 21:96–101. [PubMed: 11372069]
14. Levi AD, Sonntag VK, Dickman C, Mather J, Li RH, Berens M. Experimental Neurology. 1997; 143:25–36. [PubMed: 9000443]
15. Lewis ML, Moriarity DM, Campbell PS. Journal of Cellular Biochemistry. 1993; 51:265–273. [PubMed: 8501128]
16. Yu X, Botchwey EA, Levine EM, Pollack SR, Laurencin CT. Proceedings In Natl. Acad of Sciences. 2004; 101(3):11203–11208.
17. Lin HJ, O'Shaughnessy TJ, Kelly J, Ma W. Developmental Brain Research. 2004; 153(2):163–173. [PubMed: 15527884]
18. Valmikinathan C, Tian J, Wang J, Yu X. Journal of Neural Engineering. 2008; 5:422–432. [PubMed: 18971515]
19. Fu K, Pack DW, Klibanov AM, Langer R. Pharmaceutical Research. 2000; 17(1):100–106. [PubMed: 10714616]
20. Ozkan S, Kalyon DM, Yu X, McKelvey CA, Lowinge M. Biomaterials. 2009; 30(26):4336–4347. [PubMed: 19481253]
21. Sangsanoh P, Waleetorncheepsawat S, Suwantong O, Supaphol P. Biomacromolecules. 2007; 8(5): 1587–1594. [PubMed: 17429941]
22. Pierucci A, De Duek EAR, De Oliveira ALR. Tissue Engineering - Part A. 2008; 14(5):595–606. [PubMed: 18399734]
23. Kong L, Ao Q, Gong K, Wang X, Lu G, Gong Y, Zhang X. J Biomater Appl. 2007; 22:223–39. [PubMed: 17255157]
24. Frerichs O, Fansa H, Schicht C, Wolf G, Schneider W, Keilhoff G. Microsurgery. 2002; 22(7): 311–315. [PubMed: 12404350]
25. Fonner JM, Forciniti L, Nguyen H, Byrne JD, Kou YF, Syeda-Nawaz J, Schmidt CE. Biomedical Materials. 2008; 3(3):034124. [PubMed: 18765899]
26. Pennisi CP, Sevcencu C, Dolatshahi-Pirouz A, Foss M, Hansen JL, Larsen AN, Zachar V, Besenbacher F, Yoshida K. Nanotechnology. 2009; 20(38):385103. [PubMed: 19713588]
27. Liao H, Andersson AS, Sutherland D, Petronis S, Kasemo B, Thomsen P. Biomaterials. 2003; 24:649–654. [PubMed: 12437959]
28. Erisken C, Kalyon DM, Wang H. Biomaterials. 2008; 29(30):4065–4073. [PubMed: 18649939]
29. Sikavitsas VI, Bancroft GN, Mikos AG. Journal of Biomedical Materials Research. 2002; 62(1): 136–148. [PubMed: 12124795]
30. Meretoja VV, Malin M, Seppälä JV, Närhi TO. Journal of Biomedical Materials Research - Part A. 2009; 89(2):317–325. [PubMed: 18431787]
31. Ohyabu Y, Tanaka J, Ikada Y, Uemura T. Materials Science and Engineering C. 2009; 29(4): 1150–1155.
32. Botchwey EA, Pollack SR, Levine EM, Laurencin CT. Journal of Biomedical Materials Research. 2001; 55(2):242–253. [PubMed: 11255176]
33. Vunjak-Novakovic G, Martin I, Obradovic B, Treppo S, Grodzinsky AJ, Langer R, Freed LE. Journal of Orthopaedic Research. 1999; 17(1):130–138. [PubMed: 10073657]
34. Ju ZH, Liu TQ, Ma XH, Cui ZF. Biomedical And Environmental Sciences. 2006; 19:163–168. [PubMed: 16944770]
35. Begley CM, Kleis SJ. Biotech and Bioengineering. 2000; 70(1):32–40.

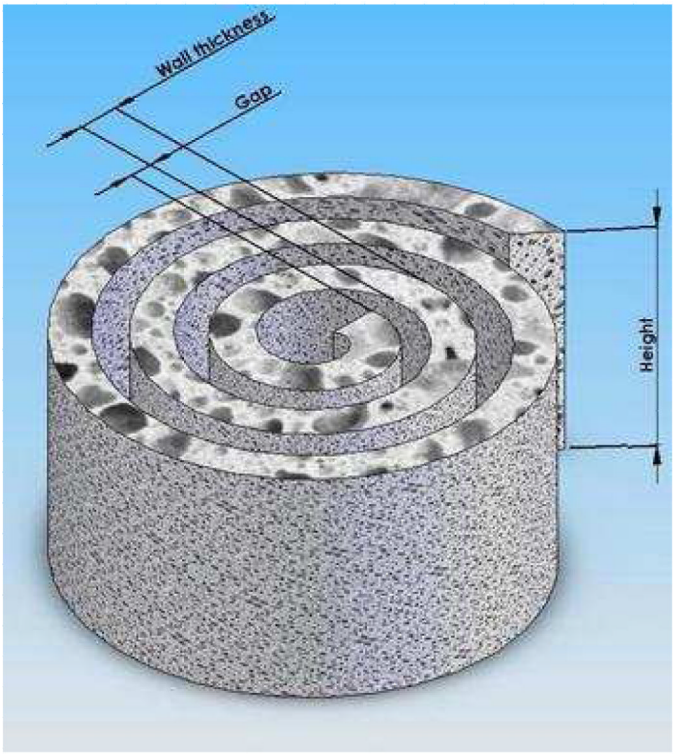

FIGURE 1.

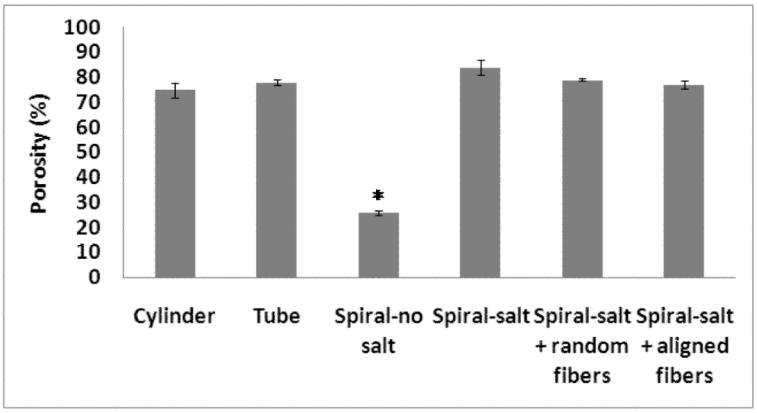

FIGURE 2.

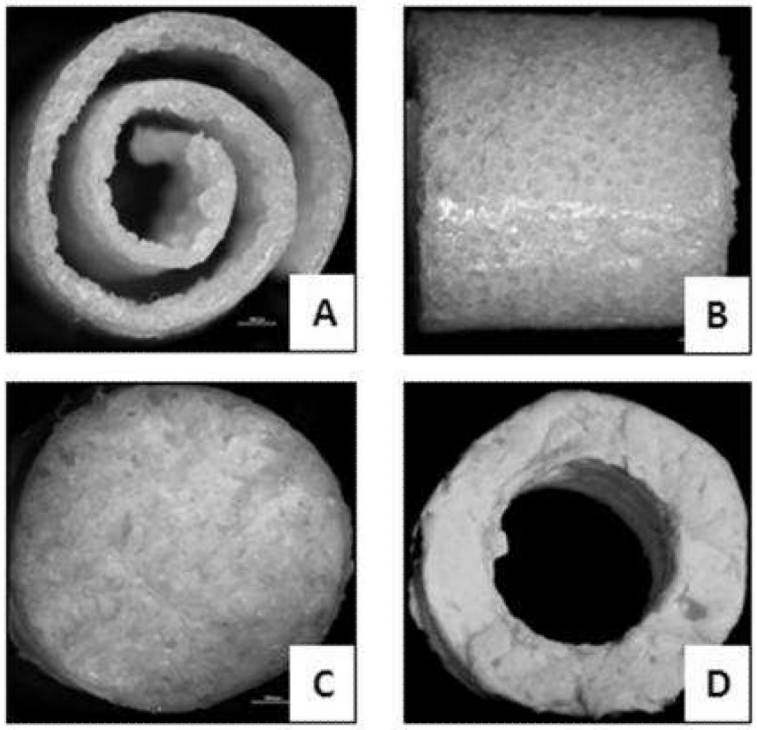

FIGURE 3.

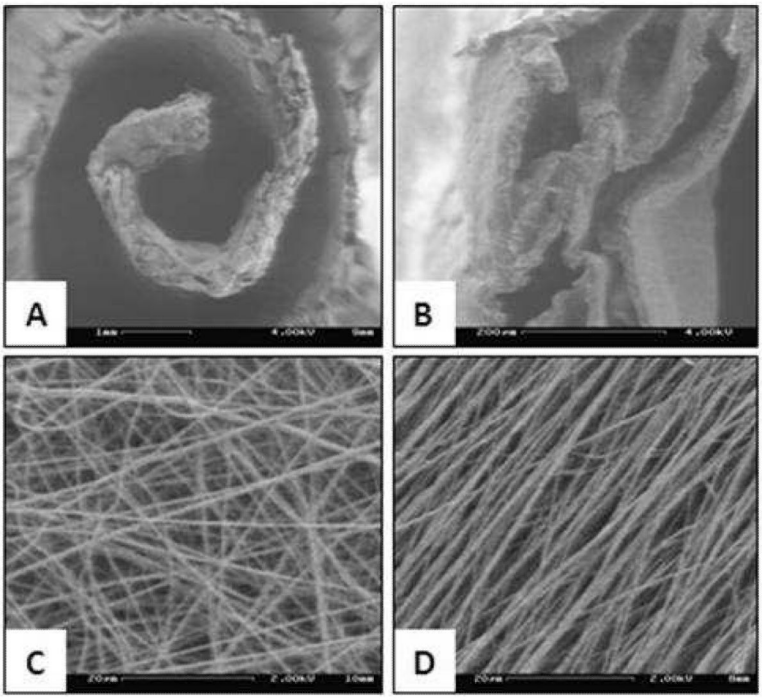

FIGURE 4.

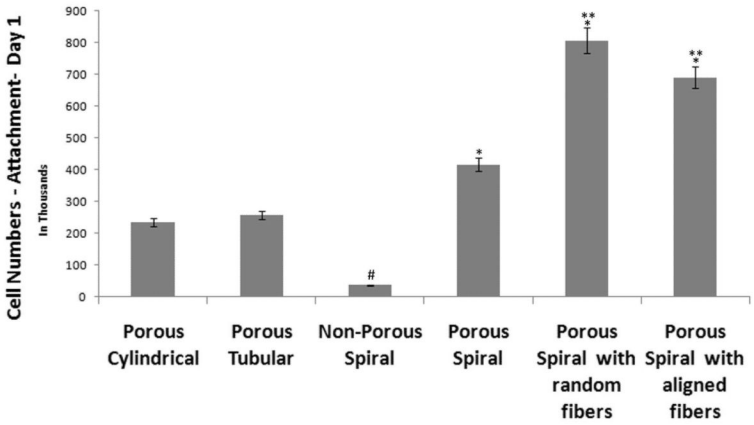

FIGURE 5.

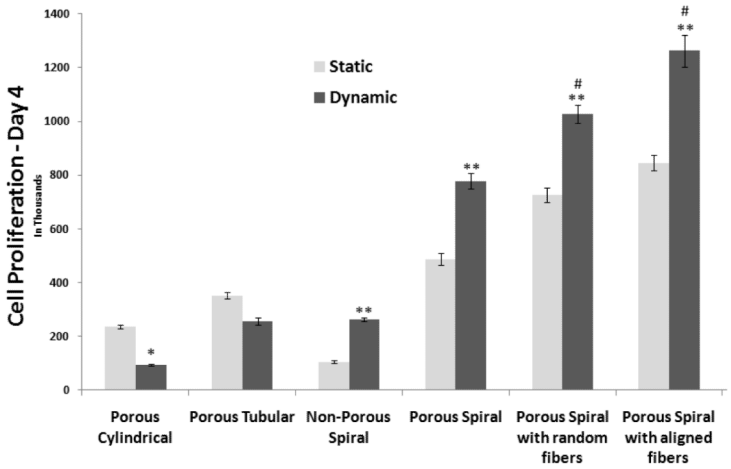

FIGURE 6.

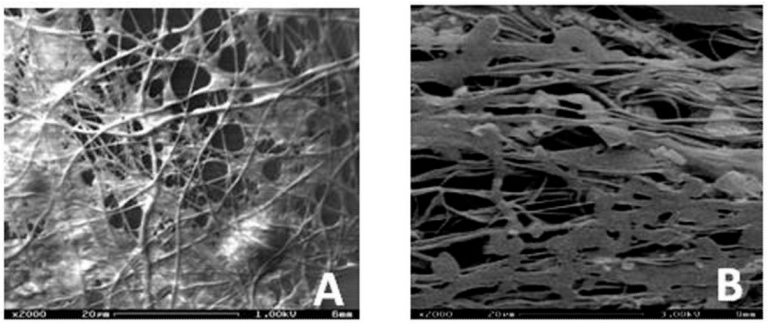

FIGURE 7.

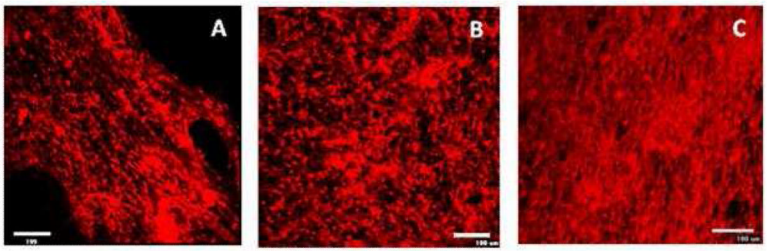

FIGURE 8.